Supporting Information

Ab-initio positioning of the valence and conduction bands of bulk photocatalysts: Proposition of absolute reference energy

Tilak Das†*, Xavier Rocquefelte‡*, and Stéphane Jobic

Université de Nantes, CNRS, Institut des Matériaux Jean Rouxel, IMN, F-44000, Nantes, France

†Current Address: Dipartimento di Scienza dei Materiali, Università degli Studi Milano-Bicocca, Via Roberto Cozzi, 55, Milano - 20125, Italy; E-mail: tilak.das@unimib.it

‡Current Address: Institut des Sciences Chimiques de Rennes UMR 6226, Université de Rennes 1, Campus de Beaulieu, 35042 Rennes, France; E-mail: xavier.rocquefelte@univ-rennes1.fr

ABSTRACT: Finding absolute reference energy from first-principles calculations to align redox positions of valence band top and hence conduction band bottom of bulk inorganic photocatalysts is still a challenge. A theoretical methodology is proposed herein based on first-principles calculations using state-of-art hybrid density functional theory from Heyd-Scuseria-Ernzerhof. Both oxides and non-oxides materials, known for their potential capability for photocatalysis *i.e.* rutile- and anatase TiO_2, wurtzite ZnO, rutile SnO_2, blende phase of GaP, GaAs, InP, ZnTe, CdS, CdSe, and SiC, have been studied. The calculated band-edges around the fundamental band-gap of these compounds are realigned, reference to the corrected vacuum energy level from the probe's core energy state *i.e.* the $1s^2$ state of an unreactive helium atom. Calculated ab-initio positioning of valence and conduction band extrema are compared to the available experimental data, and our prediction is best fitted within mean absolute error of 0.2 eV.

Table of Contents:

Section S1: Computational Details

All First-principles calculations were performed using the PBE (Perdew-Burke-Ernzerhof) version of the GGA (Generalized Gradient Approximation)[1] exchange-correlation in energy functional alone with PAW (Projector Augmented Wave)[2] basis as implemented in pseudopotential based DFT code VASP (Vienna Ab-initio Simulation Package)[3,4]. The wave-function cut-off was set at 650 eV during the expansion of the plane-wave basis-set of the valence electrons. In the valence of Sn, total 14 electrons was considered Sn[$4d^{10}5s^25p^2$]; 12 electrons for Ti[$3s^23p^64s^23d^2$], Cd[$4d^{10}5s^2$], Zn[$3d^{10}4s^2$]; 13 electrons for In[$4d^{10}5s^25p^1$], Ga[$3d^{10}4s^24p^1$]; 4 electrons for C[$2s^22p^2$] and Si[$3s^23p^2$]; 6 for O, S, Se, Te[ns^2np^4] with n = 2,3,4,5 respectively and 5 electrons for P, As[ms^2mp^3], with m=3,4 respectively.

Using the conjugate gradient algorithm the self-consistency was ensured with energy convergence until reached 10^{-8} eV. The DFT static calculations were done with tetrahedron methods, to get density of states (DOS) with an energy resolution of 0.01 eV and Gaussian broadening 0.1 eV. The slabs were cut from the experimental bulk structure with non-polar surface terminations and chemically stoichiometric. The Brillouin zone integration was done using Monkhorst Pack sampling with an in-plane k-mesh 8×8 for all models in PBE-GGA level depending upon the choice of the in-plane lattice vectors or surface and 1× for out-of-plane lattice vector of the slab. The HSE hybrid calculations[5,6] were done only using the VASP package, with Hartree-Fock exact exchange (α) varying from 0.00 to 1.00 for four different points *i.e.* α = 0.00, 0.20, 0.25 and 0.73 with screening distance fixed to 0.20$Å^{-1}$. The previously used *k*-mesh is reduced to 4×4 for HSE calculations for in-plane and 1× for out-of-plane. All the ground state static DFT calculated data also verified from plane-wave based full-potential package WIEN2K[7] with considering the same level of accuracy on their different parameter choices *i.e.* energy cut-off, k-mesh and atomic radii.

The hybrid functional is constructed based on the following formulation from PBE-GGA functional based correlation E_c^{GGA} with fraction of exchange is replaced by Hartree-Fock exchange, E_x^{HF}. The following eq. 1 is applied here,

$$E_{xc} = \alpha E_x^{HF} + (1- \alpha)E_x^{GGA} + E_c^{GGA}$$

Section S2: He-Slab Models

The He-Slab model was generated from the standard slab-model by additional Helium atom at the center of the vacuum. For example few test models are represented within the Figure S1 for clarity. The details of the used all eleven slab-models are given in Table S1.

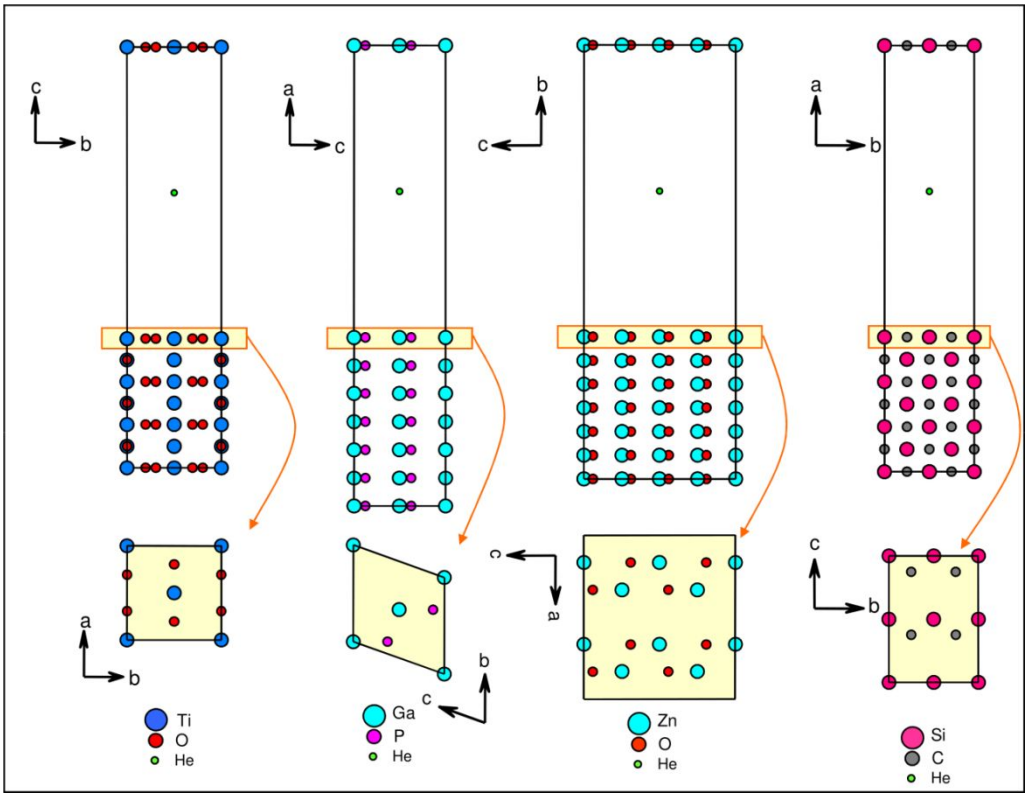

Figure S1. The conventional layer-vacuum models used for the computations, for example using rutile-TiO_2, wurtzite-ZnO, blende-GaP and SiC is shown in the above figure, respectively from left to right panels. The He-atom is denoted with the green filled circles at the centre (center of vacuum) of the each model.

Table S1. The structural details of He-Slab supercell models with 20Å vacuum and He atom at the middle of the vacuum. The bulk phase structural parameters are used and their corresponding references are given in last column.

He-Slab Model	a(Å)	b(Å)	c(Å)	Vacuum direction	Surface Normal to Vacuum	Reference
SnO_2	6.70	6.70	29.56	<001>	(110)	[8]
R-TiO_2	6.50	6.50	28.88	<001>	(110)	[9]
CdS	32.37	7.14	7.14	<100>	(110)	[10]
A-TiO_2	7.57	31.35	9.51	<010>	(010)	[11]
ZnO	11.25	29.75	10.41	<010>	(110)	[12]
SiC	29.25	6.16	8.72	<100>	(110)	[13]
CdSe	32.89	7.44	7.44	<100>	(110)	[14]
InP	32.45	7.19	7.19	<100>	(110)	[15]
GaP	31.56	6.67	6.67	<100>	(110)	[16]
GaAs	31.99	6.92	6.92	<100>	(110)	[17]
ZnTe	32.95	8.63	6.10	<100>	(110)	[18]

Section S3: Dependence of Vacuum Width vs. DFT Functional

The vacuum width of the He-slab model is checked with the different DFT energy functional with the choice of Hartree-Fock exact-exchange (α) for 0% and 25% in addition with GGA exchange amount. In the Figure S2, the plot of local atomic potential is represented for GaP He-slab model. Here, we have used 7-layers of material separated by 20Å of vacuum along <100> direction. As we can see, the calculated vacuum energy level and the energy He($1s^2$) has reached reasonable convergence, except the impact of exchange amount increases the value of the atomic core potential at 7 layers (bottom panel).

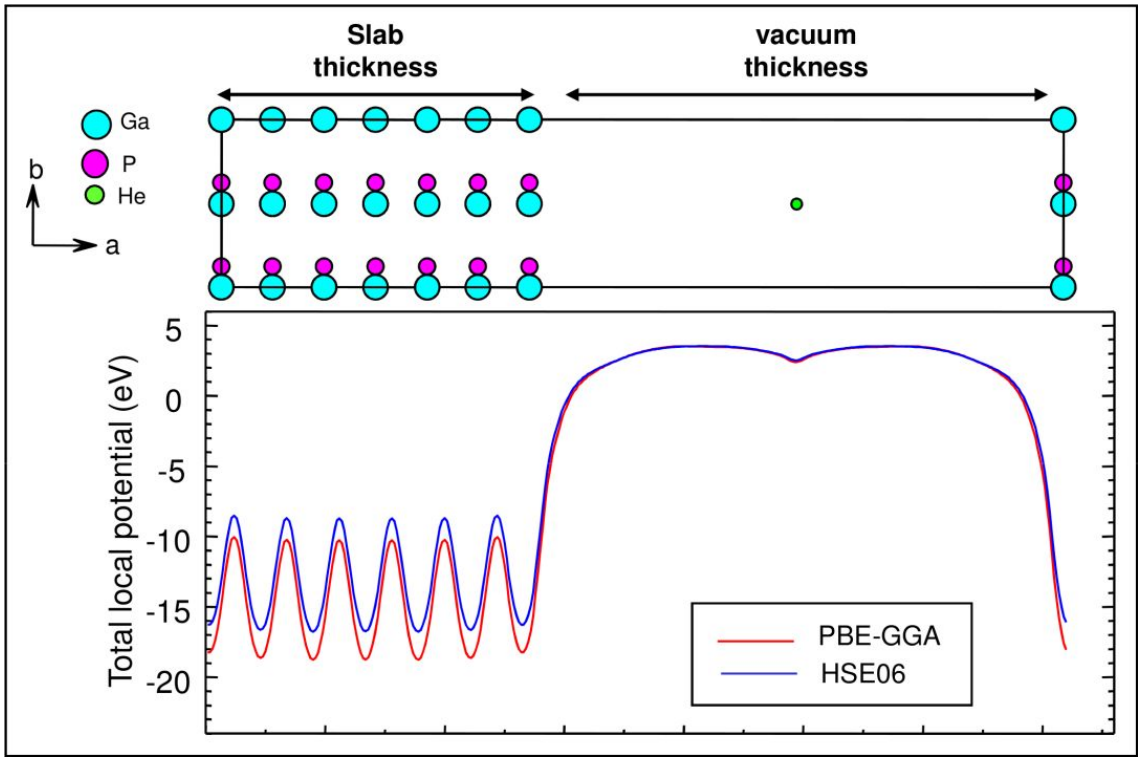

Figure S2. The calculated local potential (bottom panel) is shown of the blende-GaP He-slab model (top panel). The calculations are done using PBE-GGA (α=0.00) and HSE06 (α=0.25) exchange energy functional using VASP package as shown in the bottom panel.

Section S4: Energy of He(1S²) vs. Vacuum Width Check

In this step, we are interested to cross check the accuracy of the choice of finite 20Å vacuum using the test case of GaP He-slab model, and ground state DFT functional PBE-GGA. Thus, we have plotted the energy difference of the He(1s²) energy level and vacuum energy level calculated from the same calculation vs. the different vacuum width from 8-100Å. The result is shown in the Figure S3. It is clear that the true convergence reached at 40Å and thus the choice of 20Å vacuum led to ~ 0.1 eV of energy error bar to the calculated vacuum level.

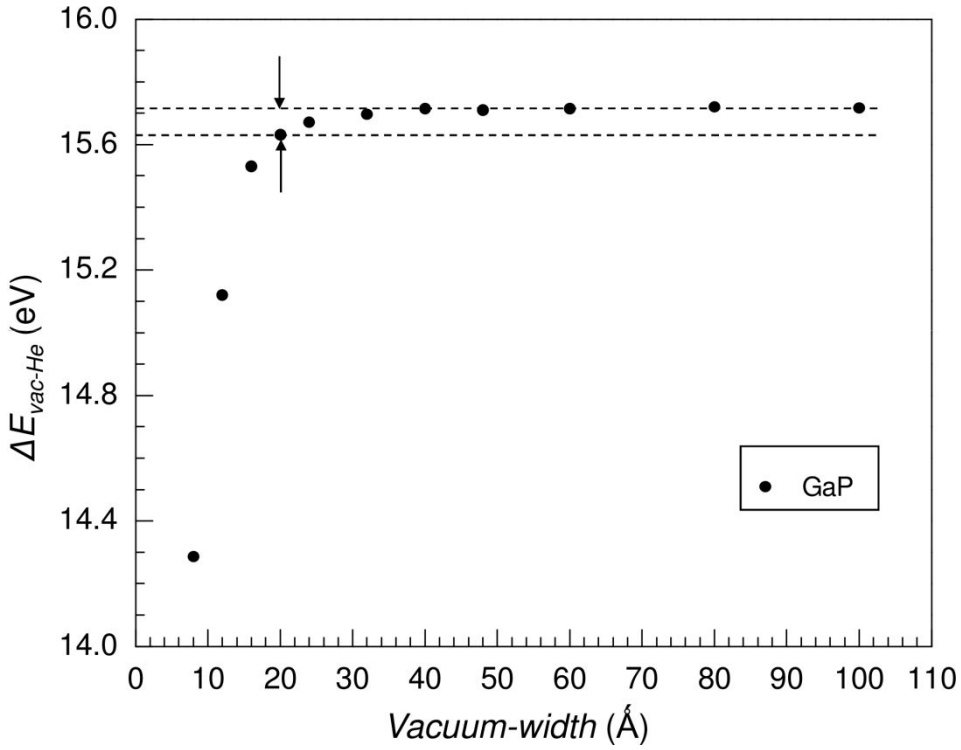

Figure S3. The calculated energy difference of He(1s²) and corresponding vacuum energy level ($\Delta E_{vac\text{-}He}$ in eV) vs. *Vacuum-width* (in Å) of the blende-GaP case, using PBE-GGA energy functional.

Section S5: Layer Thickness vs. Vacuum Width Check

In this section, the layer width is checked depending on the cell dimension alone the vacuum direction. We have used the test case of the rutile TiO_2 and PBE-GGA calculation on the He-Slab model. In the Figure S4, the difference of the planner average of the local atomic potential (blue dashed line) and calculated value of vacuum energy level from the same 7 layers (top panel) or 15 layers (bottom panel) is shown. Thus, it is clear that the use of the 7 layer of material, along with 20Å of vacuum, even for the oxides it is quite reasonable.

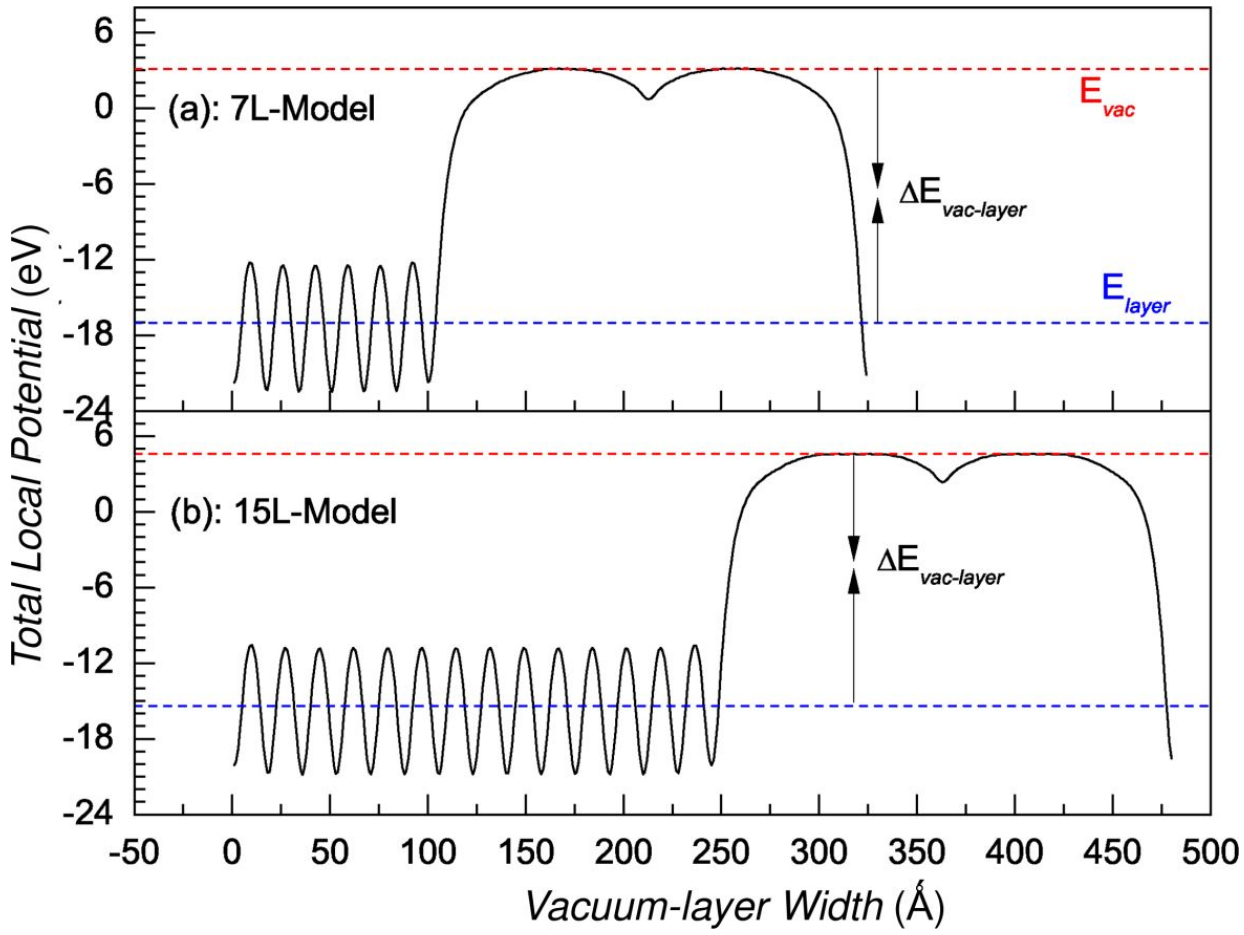

Figure S4. The calculated energy difference of planar average total local potential and corresponding vacuum energy level ($\Delta E_{vac\text{-}layer}$ in eV) vs. *Vacuum-layer-width* (in Å) of the R-TiO_2 case for check, using PBE-GGA energy functional. On the top panel the 7-layer and at the bottom panel the 15-layer model's data are shown.

Section S6: Atomic Core Potential vs. Exact-exchange in DFT Functional

In this section, we have evaluated the dependence of atomic core potential of constituent atoms and energy of the He($1s^2$) in a He-Slab model, along with 20Å vacuum with the variation of the Hartree-Fock parameter, α from 0.0%-75.0% for exact-exchange within HSE hybrid DFT calculations for test case GaP. In the top panel of Figure S5, the core potential of Ga, P, and He is shown and the total energy of the He($1s^2$) vs. α parameter. We see in both cases, there is a linear dependence of these quantities with α parameter.

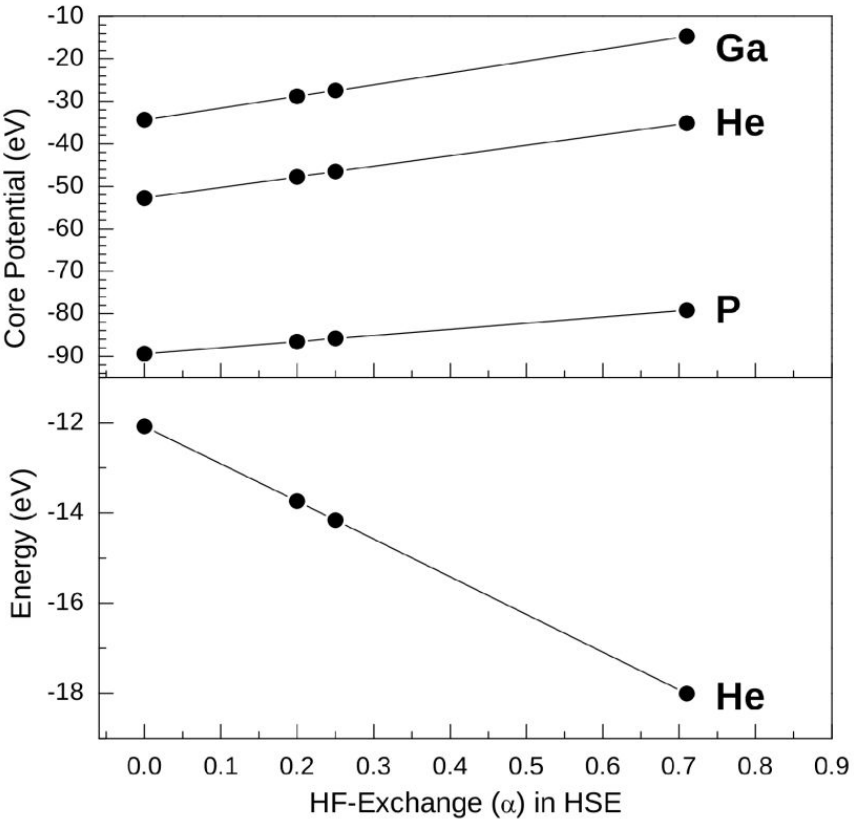

Figure S5. The calculated average core potential of Ga, P, and He atoms in the He-GaP model, and He($1s^2$) energy level in the top and bottom panel, respectively vs. different Hartree-Fock exact exchange α values.

Section S7: Energy of He(1s²) vs. Exact-exchange of DFT Functional

Since we have seen, the impact of the He(1s²) energy level is very crucial for the detection of the error amount in the calculated vacuum level for individual He-Slab approach, thus its variation was checked w.r.t. the value of the Hartree-Fock (HF) exact exchange, α through the hybrid calculation using HSE functional (cf. Figure S6). Indeed, this was done for the all eleven compounds, with the knowledge of the linear dependence of the He(1s²) energy (cf. Figure S5) vs. α parameter from the extrapolation at α = 0.0 and 0.25 values calculated data.

At ground state DFT level (α = 0.00) we have seen that in all models, the value of He(1s²) is just around the -15.64 eV compared to the experimental data of He ionization energy -24.59 eV. It is obvious that a large value of the exact-exchange is needed for the description of the He(1s²) energy and this is different for the different materials He-slab model. This error amount was also incorporated within the prediction.

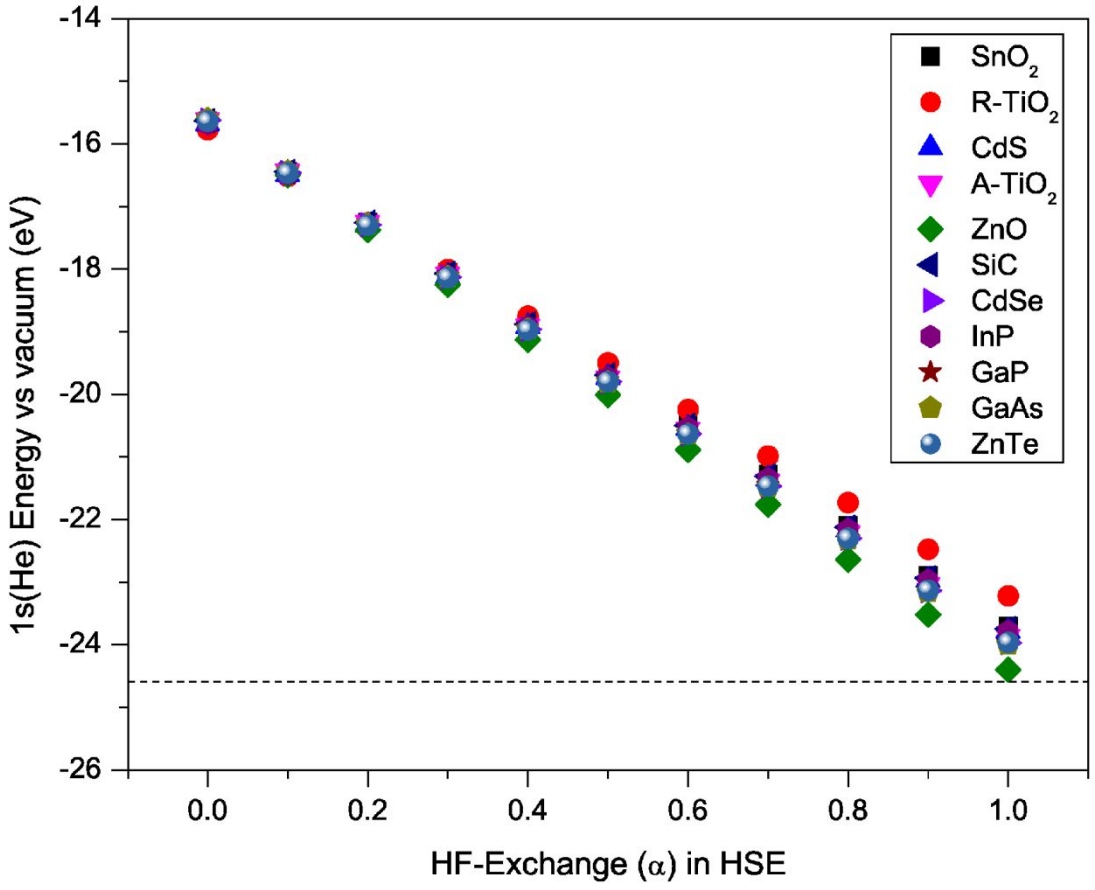

Figure S6. Linear extrapolation of the He(1s²) energy level vs. different values of α, between 0.00 to 1.00 following the calculated values of the He(1s²) at α=0.00 and 0.25 for exact-exchange. The black dashed line is the experimental value of the corresponding energy level.

Section S8: Energy of He(1s²) vs. He-He Interaction Distance in Models

Finally, in this section the nature of the He-He interaction is checked which is coming from the He-Slab approach due to the choice of finite in-plane lattice parameters of the slab models. In this Figure S7, the variation of the He(1s²) energy level is shown considering He atom in a cubic box with cell size varying 5-30Å at the PBE-GGA ground state DFT level. The trend remain unchanged even with the hybrid DFT level at α = 0.25, as shown inset of the Figure S7. Actual convergence of the He-He interaction was achieved at distance ~ 30Å compared to our finite in-plane lattice size choice for the different materials as shown in Table S2. With a Lorentzian fit to the calculated data the error amount was extract from the prediction.

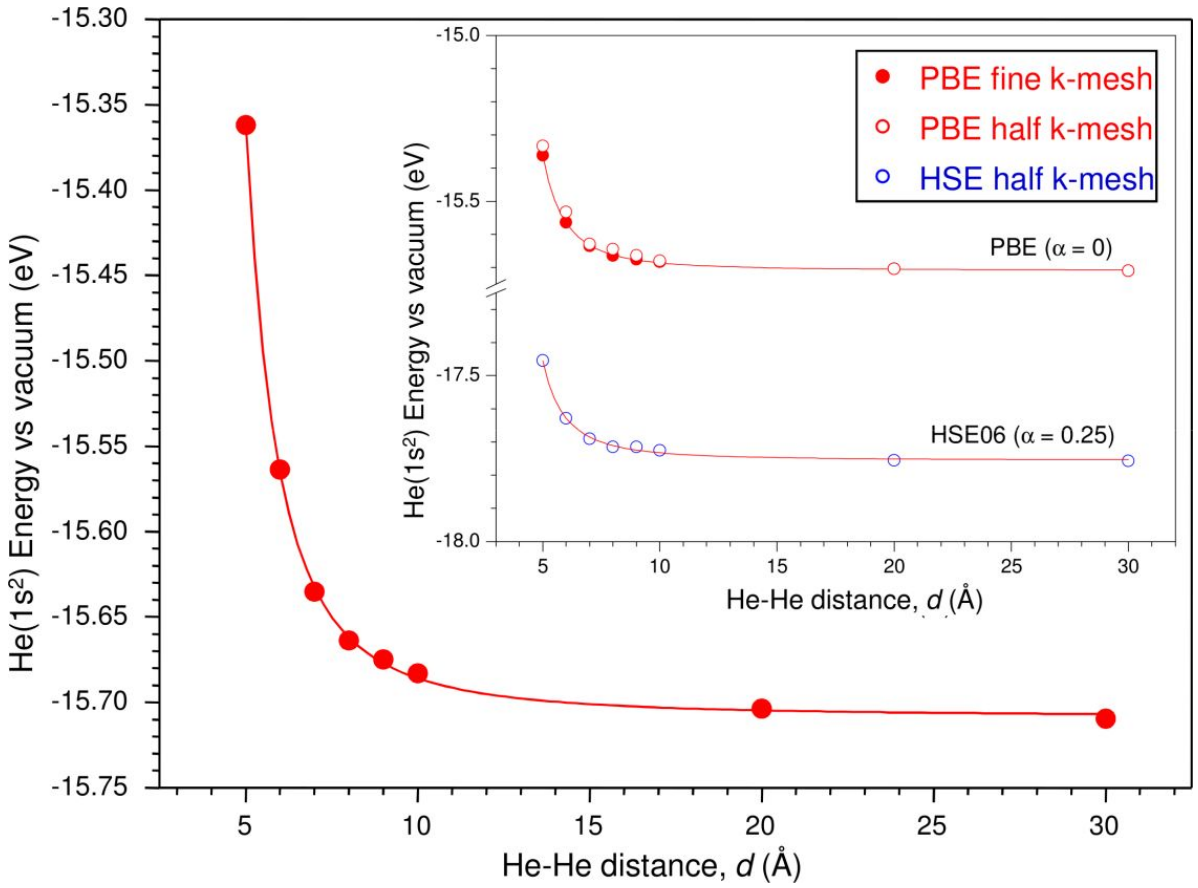

Figure S7. The evolution of the He(1s²) energy level w.r.t. the He-He distance (*d*) using a cubic box starting from 5-30Å cell size. The circles (filled or empty) are data from a PBE-GGA functional (α = 0.00), and the empty blue one (inset) from HSE06 functional (α = 0.25). The red solid line is Lorentz fit for each plots.

Table S2. The evolution of the error coming in estimation of He(1s2) energy level w.r.t. the He-He distance (*d*) due to the finite He-He distance in the He-Slab approach.

He-Slab Model	Lowest He-He Distance (Å)	Error Value (eV)
SnO_2	6.70	-0.09
R-TiO_2	6.50	-0.10
CdS	8.25	-0.04
A-TiO_2	7.57	-0.06
ZnO	10.41	-0.02
SiC	6.16	-0.13
CdSe	8.59	-0.04
InP	8.30	-0.04
GaP	7.70	-0.05
GaAs	7.99	-0.05
ZnTe	6.11	-0.13

References

[1] J. P. Perdew, K. Burke, and M. Ernzerhof, *Phys. Rev. Lett.***1996**, *77*, 3865-3868.

[2] G. Kresse and D. Joubert, *Phys. Rev.B* **1999**, *59*, 1758-1775.

[3] G. Kresse and J. Hafner, *Phys. Rev.B* **1993**, *47*, 558-561.

[4] G. Kresse and J. Furthmuller, *Phys. Rev.B* **1996**, *54*, 11169-11186.

[5] J. Heyd, G. E. Scuseria, and M. Ernzerhof, *J. Chem. Phys.* **2003**, *118*, 8207-8215.

[6] J. Heyd, G. E. Scuseria, and M. Ernzerhof, *J. Chem. Phys.* **2006**, *124*, 219906-1.

[7] P. Blaha, K. Schwarz, G. K. H Madsen, D. Kvasnicka, and J. Luitz, *WIEN2K* (Eds. K. Schwarz), Technische Universitiät Wien, Vienna, **2001**.

[8] W. H. Baur and A. A. Khan, *Acta. Cryst. B* **1971**, *27*, 2133.

[9] R. Restori, D. Schwarzenbach, and J. R. Schneider, *Acta. Cryst. B* **1987**, *43*, 251.

[10] D. Rodic, V. Spasojevic, A. Bajorer, and P. Oennerud, *J. Magnetism Magnetic Mater.* **1996**, *152*, 159.

[11] M. Horn, C. F. Schwerdtfeger, and E. P. Meagher, *Zeitschrift fuer Kristallogeometrie, Kristallphysik, Kristallchemie* **1972**, *136*, 273.

[12] W. Bragg, *Transac. Faraday. Soc.* **1932**, *28*, 522.

[13] T. Kawamura, *Mineral. J.* **1965**, *4*, 333.

[14] M. P. Kulakov, I. V. Bayakina, and N. N. Kholesnikov, *Inorg. Mater.***1989**, *25*, 1386.

[15] A. G. Thompson, J. E. Rowe, and M. Rubenstein, *J. Appl. Phys.* **1969**, *40*, 3280.

[16] P. Deus, U. Voland, and H. A. Schneider, *Acta. Cryst.***1958**, *11*, 369.

[17] A. W. Stevenson, *Acta. Cryst. A* **1994**, *50*, 621.

[18] J. L. Baudour, M. M. Granger, and L. Toupet, *J. Phys. Chem. Sol.* **1989**, *50*, 309.